

## S1 Optical models and parametrisations

The following sections give descriptions of the various optical models used in this analysis. Only the Liu- $E_{\text{Abs}/\text{Sca}}$  parametrisation is used to convert from the single-particle light scattering and  $M_{\text{BC}}$  measured by the SP2 into MR. This process is described in Sect. 4.1, and this set of calculations is performed using a value of  $m_{\text{BC}} = (2.26 - 1.26i)$  at the SP2 instrument wavelength of 1064 nm. All the models are then used to convert the 2D distributions of MR vs  $M_{\text{BC}}$  into bulk absorption at visible wavelengths, using the range of  $m_{\text{BC}}$  listed in Table S1.

**Table S1.** List of the different values of  $m_{\text{BC}}$  used in this study

$m_{\text{BC}}$	Reference
(1.75 - 0.63 <i>i</i> )	(Bond and Bergstrom, 2006)
(1.80 - 0.67 <i>i</i> )	(Bond and Bergstrom, 2006)
(1.85 - 0.71 <i>i</i> )	(Bond and Bergstrom, 2006)
(1.90 - 0.75 <i>i</i> )	(Bond and Bergstrom, 2006)
(1.95 - 0.79 <i>i</i> )	(Bond and Bergstrom, 2006)
(2.26 - 1.26 <i>i</i> )	(Moteki et al., 2010)

### S1.1 Coated sphere

- 5 The core/shell Mie model considers internally mixed soot particles as consisting of a BC core coated in a non-BC shell, in a morphology of two concentric spheres. It has been implemented in some climate models to calculate bulk scattering and absorption (e.g. Matsui et al., 2013). For calculating absorption, we use two implementations of the core/shell Mie model. For the first we use the core/shell Mie model in its standard form to calculate absorption, and divide by mass to get  $\text{MAC}_{\text{CS}}$ , the MAC calculated using the core/shell Mie model. We also use an additional implementation, termed CS- $E_{\text{Abs}}$  where the
- 10 core/shell model is used to calculate  $E_{\text{Abs}}$  only, and this is then multiplied by the MAC of uncoated BC to give the coated MAC. The best estimate is provided by Bond and Bergstrom (2006), who summarised previous literature and reported an average value of  $7.5 \text{ m}^2 \text{ g}^{-1}$  at 550 nm (with AAE = 1), which we refer to as  $\text{MAC}_{\text{BB}}$ . The MAC of internally-mixed BC is then calculated by multiplying  $E_{\text{Abs}}$  by  $\text{MAC}_{\text{BB}}$ .

### S1.2 Homogeneous grey sphere models

- 15 We use the term "grey sphere" to refer to any model that approximates particles as a homogeneous sphere with a single effective refractive index ( $m_{\text{Eff}}$ ). This approach was described by Stier et al. (2007) and is still used in some climate models (e.g. Bellouin et al., 2013) as it is less computationally expensive than more complex schemes, and requires less constraint. Several mixing rules are possible to calculate the effective refractive index by combining the different components.

## Volume mixing

- 20 Here the weighted mean refractive index is calculated, with weights determined by the volume fraction of each component

$$m_{\text{Eff}} = \sum_{i=1}^{\infty} (F_i m_i)$$

where  $F_i$  and  $m_i$  are the volume fraction and refractive index for component  $i$ .

The components we considered are BC, OA, ammonium nitrate, and ammonium sulphate, although the non-BC components are all assumed to have the same refractive index.

## Bruggeman mixing rule

- 5 The Bruggeman mixing rule computes the effective electric permittivity ( $\epsilon_{\text{Eff}} = m_{\text{Eff}}^2$ ) of two components distributed symmetrically. The two components are BC and non-BC, which is a sum of OA, ammonium nitrate, and ammonium sulfate. The permittivity of the non-BC components was calculated using volume mixing.  $\epsilon_{\text{Eff}}$  is then calculated using

$$\epsilon_{\text{Eff}} = \frac{b + \sqrt{8\epsilon_{\text{BC}}\epsilon_{\text{non-BC}} + b^2}}{4}, b = (2F_{\text{BC}} - F_{\text{non-BC}})\epsilon_{\text{BC}} + (2F_{\text{BC}} - F_{\text{non-BC}})\epsilon_{\text{non-BC}},$$

where  $\epsilon_{\text{BC}}$  and  $\epsilon_{\text{non-BC}}$  are the electric permittivities and  $F_{\text{BC}}$  and  $F_{\text{non-BC}}$  are the volume fractions of the two components

- 10 (Markel, 2016, eq. (30)).

## Maxwell-Garnett mixing rule

The Maxwell-Garnett mixing rule considers small particles of one component (BC) dispersed evenly in a host medium (non-BC). The non-BC components were summed together as in the Bruggeman mixing rule, and  $\epsilon_{\text{Eff}}$  is calculated using

$$\epsilon_{\text{Eff}} = \left[ 1 + 3F_{\text{BC}} \left( \frac{\epsilon_{\text{BC}} - \epsilon_{\text{non-BC}}}{\epsilon_{\text{BC}} + 2\epsilon_{\text{non-BC}}} \right) / \left( 1 - F_{\text{BC}} \left( \frac{\epsilon_{\text{BC}} - \epsilon_{\text{non-BC}}}{\epsilon_{\text{BC}} + 2\epsilon_{\text{non-BC}}} \right) \right) \right]$$

- 15 as given by (Bohren and Huffman, 1983, eq. (8.50)).

## S1.3 parametrisations

### The Liu- $E_{\text{Abs/Sca}}$ parametrisation

- Liu et al. (2017) use an approach that applies an empirical correction to the core/shell Mie model. They compared SP2 measurements of  $E_{\text{Sca}}$ , the scattering enhancement due to coatings, to  $E_{\text{Sca,CS}}$ , the equivalent scattering enhancement at 1064 nm
- 20 for a particle with the same mass and composition but in a concentric core/shell morphology. Liu et al. (2017) based empirical fits to ambient measurements from several locations around the world, and a laboratory study using both fresh and aged diesel soot. Particles of known mass were selected by a centrifugal particle mass analyser (CPMA), and measurements were made of single-particle scattering, as well as bulk properties such as MAC.  $E_{\text{Abs}}$  and  $E_{\text{Sca}}$  were also determined by comparing measurements of untreated particles to those passed through a catalytic stripper heated to 400°C designed to remove any non-BC
- 25 material. Liu et al. (2017) then designed a parametrisation based on an empirical correction to the core/shell Mie model using an internally mixed fraction parameter ( $F_{\text{in}}$ ), which is colloquially known as the ‘core/shell-ness’. For low values of MR, BC and non-BC behave optically like externally-mixed spheres. For high values of MR, the particles behave as core/shell particles,

and there exists a transition zone for particles partway between these two regimes. Liu et al. (2017) then define  $E_{\text{Abs}}$  and  $E_{\text{Sca}}$  as

$$30 \quad E_{\text{Abs}} = E_{\text{Abs,CS}} \times F_{\text{in}} + (1 - F_{\text{in}}) \times 1,$$

$$E_{\text{Sca}} = E_{\text{Sca,CS}} \times F_{\text{in}} + (1 - F_{\text{in}}) \times 1,$$

$$\text{where } F_{\text{in}} = \begin{cases} 0, & \text{if } \text{MR} < 1.5 \\ 0.57 \times \text{MR} - 0.74, & \text{if } 1.5 \leq \text{MR} < 3 \\ 1, & \text{if } \text{MR} \geq 3. \end{cases}$$

It is implicitly assumed that  $E_{\text{Abs}}$  and  $E_{\text{Sca}}$  behave in a similar manner using the same values of  $F_{\text{in}}$ , but the parametrisation is  
 5 based on measurements of  $E_{\text{Sca}}$  at 1064 nm. To calculate the coated MAC, we multiplied the calculated  $E_{\text{Abs}}$  by  $\text{MAC}_{\text{BB}}$ .

### The Wu- $E_{\text{Abs}}$ parametrisation

Wu et al. (2018) made an empirical fit to the bulk  $E_{\text{Abs}}$  of simulated BC particles of different mixing states. In their simulation, bare BC particles were generated by diffusion limited aggregation, where BC monomers stick together to form fractal aggregates. Coating material was then added to the surface of these aggregates, in a manner intended to simulate condensation  
 10 of secondary material onto the soot, as well as coagulation with pre-existing liquid particles resulting in partial encapsulation, and complete encapsulation for higher values of MR. The optical properties of these particles were then calculated using the superposition T-matrix method, averaged for different orientations of the particles, and using a wavelength-dependent  $m_{\text{BC}}$  (Chang and Charalampopoulos, 2006). Their empirical fit for  $E_{\text{Abs}}$  took the form

$$E_{\text{Abs}} = 0.92 + 0.11 e^{(E_{\text{Abs,CS}} - 1.07)/0.55}.$$

15 In our implementation, we calculate  $\text{MAC}_{\text{CS}}$  on a bin-by-bin basis for the appropriate refractive indices from Chang and Charalampopoulos (2006), as well as  $\text{MAC}_{\text{CS}}$  if all the coating thicknesses were zero, then sum both and divide the total coated absorption by the total uncoated absorption.

Comparing their data to the measurements by Liu et al. (2017), Wu et al. (2018) found agreement within  $\sim 5\%$  for MAC at 532 nm, and  $\sim 20\%$  for scattering at 1064 nm, however they also used a specific wavelength-dependent BC refractive index in  
 20 this comparison. Again, as this parametrisation only gives  $E_{\text{Abs}}$ , we multiply the calculated  $E_{\text{Abs}}$  by  $\text{MAC}_{\text{BB}}$  to give the coated MAC.

### The Chak- $E_{\text{Abs}}$ and Chak-MAC parametrisations

Chakrabarty and Heinson (2018) developed a parametrisation applying discrete-dipole approximation calculations to simulated BC particles. Particles were generated in a similar manner as Wu et al. (2018). The parametrisation is described in several  
 25 different forms, and here we apply two approaches, Chak-MAC and Chak- $E_{\text{Abs}}$ . In Chak-MAC, MAC is calculated using

$$\text{MAC} = (3.6/\lambda) \left( \frac{M_{\text{tot}}}{M_{\text{BC}}} \right)^{(1/3)},$$

where  $M_{\text{tot}} = M_{\text{non-BC}} + M_{\text{BC}}$ .

In Chak- $E_{\text{Abs}}$ ,  $E_{\text{Abs}}$  is calculated as

$$E_{\text{Abs}} = \left( \frac{M_{\text{tot}}}{M_{\text{BC}}} \right)^{(1/3)} .$$

- 30 We then multiply  $E_{\text{Abs}}$  by  $\text{MAC}_{\text{BB}}$  to calculate MAC. The implication of the comparison between Chak- $E_{\text{Abs}}$  and Chak-MAC is that the MAC of uncoated BC follows the rule  $\text{MAC}_{\text{bare}} = (3.6/\lambda)$ , which produces results 13% lower than  $\text{MAC}_{\text{BB}}$ .

## S2 Correction for SP2 limited detection range

Figure S2 shows BC properties from one straight and level run on the 4 September 2017, though equivalent distributions were generated for each straight and level run during the campaign. Panel (a) shows the number mass distributions of BC cores. We do not correct for particles with BC content that is too small for the instrument to detect as these particles contain only a small fraction of the total BC mass concentration (Laborde et al., 2012b). Figure S2 (a) shows two distributions- one for all detected particles, and another for those that had a successful leading-edge only (LEO) fit to measure the scattering cross-section of BC-containing particles at 1064 nm. Of the particles that are detected, not all of them have a successful LEO fit due to the limited detection range of the scattering channel, as well as the relative importance of detector noise and saturation for different sized particles. The size-dependent ratio of these two distributions ( $F_{LEO}$ ) is shown as the black line in panel (b). For most of the BC size distribution  $F_{LEO}$  was around 70 – 80 %, decreasing sharply to zero below 0.5 fg  $M_{BC}$  at the low end, and gradually decreasing from 0.8 to  $\sim 0.5$  above around 10 fg, though this high end was noisy due to limited particles at the larger sizes.

Figure S2 (b) also shows the distribution of  $E_{Sca}$  versus  $M_{BC}$ , where  $E_{Sca}$  is the ratio of the measured scattering cross-section to Mie calculations for a bare BC core.  $E_{Sca}$  is a useful diagnostic as it gives an indication of BC mixing state that is independent of the morphology of the mixed particle. It is also unconstrained by the physical impossibility of concepts such as negative coating thickness, which arise due to the particle-by-particle variability of the measured signals. This plot shows a distribution of  $E_{Sca}$  around 100 for a 1 fg core, decreasing with size by an order of magnitude up to cores around 4 fg. There were few particles measured with  $E_{Sca}$  around 1, for bare BC cores, suggesting almost all the BC-containing particles had some degree of internal mixing. At the high and low ends of the  $M_{BC}$  distribution, where  $F_{LEO}$  dropped below 0.5, the MR distributions of the neighbouring bins were extended to complete the distribution, in proportion to the number of particles measured.

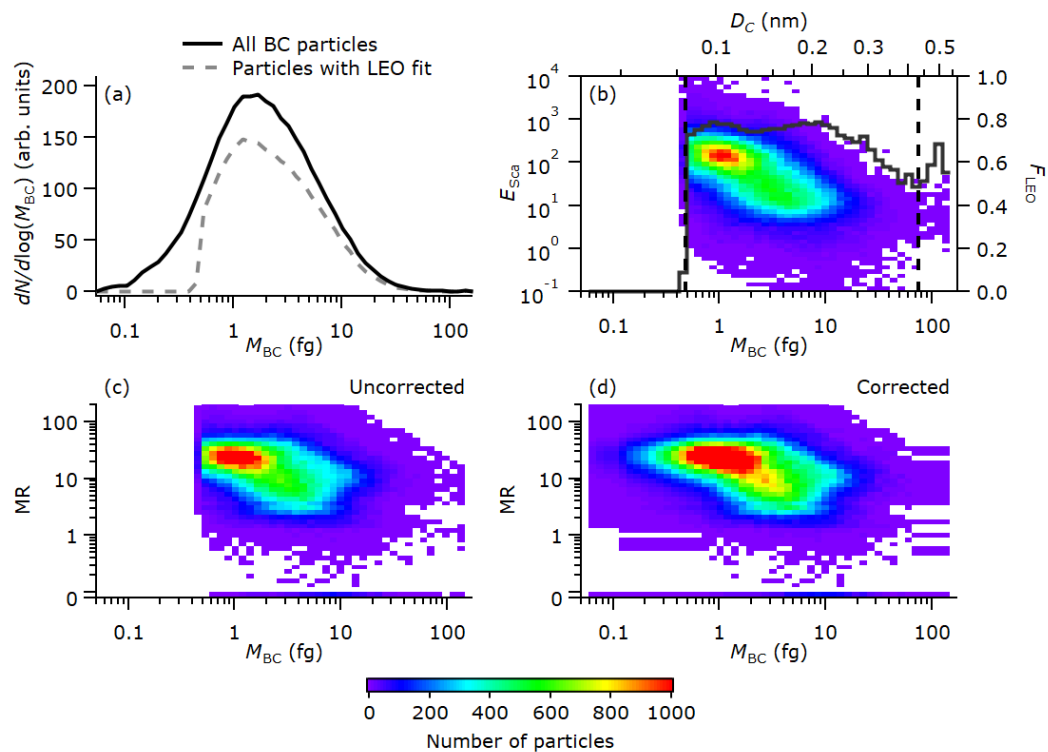


**Figure S2.** Panel (a) shows the number distribution of BC cores, both for all particles and just those with a good LEO fit. Panel (b) shows the distribution of  $E_{Sca}$  for particles of different  $M_{BC}$ , and the fraction of particles with a good LEO fit at each size. The vertical dashed lines show the bounds of the region where  $F_{LEO}$  was above 0.5. Panels (c) and (d) show the 2-D distributions of BC size and mixing state, comparing the distributions before and after correction for the limited detection of particles by the SP2 instrument.

### S3 Monte-Carlo uncertainty analysis in Mie models

The aim of this Monte-Carlo uncertainty analysis is to determine the uncertainty of parameters such as coating thickness, MAC, and AAE, that are derived using the optical codes described in Sect. S1. These uncertainties cannot be determined analytically due to the complexity of the calculation. Our approach is to use the uncertainty in the input variables to generate a scale factor ( $\kappa$ ) to represent the variability that each input variable might have if it were measured a large number of times, in this case 10000. Arrays of scale factors were generated such that the distribution of each scale factor is a Gaussian distribution centred on one, with a width of the stated uncertainty for each variable. For example, to represent the 11% uncertainty in the SP2 scattering channel, the scale factor array is made of 10000 normally distributed numbers with a mean of 1 and a standard deviation of 0.11. For each calculation, this was then used to multiply the calibration factor for the SP2 scattering channel.

The variables we considered in this analysis are the calibrations for the SP2's incandescence and scattering channels, and the concentrations of the species measured by the AMS, which are used to calculate the density and refractive index of the coatings. We do not consider the density and refractive index of the BC in these calculations. For the purposes of the inversion to determine the BC properties based on the SP2 data, the values of  $\rho_{\text{BC}} = 1.8 \text{ g cm}^{-3}$  and  $m_{\text{BC}} = (2.26 - 1.26i)$  are used for the reasons given in Sect. 4.1. Particularly when using the Liu et al. (2017) parametrisation, these are not free parameters, and previous literature provides little guidance as to what the uncertainty is on these parameters. During the forward model calculations of MAC and AAE, our analysis explicitly includes different values of  $m_{\text{BC}}$ .

Scale factors were applied for the SP2 and AMS data from one straight and level run from the aircraft measurements on 1<sup>st</sup> September. This run was chosen as it was relatively short (4 minutes) so the calculation is quicker to run.

#### SP2 calibrations

The SP2's scattering channel was calibrated using nebulised 200 nm PSLs, and the measured modal signal varied by  $\pm 11\%$  throughout the campaign. The incandescence channel is used to determine single particle BC mass, and this channel was calibrated using nebulised Aquadag, which was selected by mass using a centrifugal particle mass analyzer (CPMA), and corrected as described by Laborde et al. (2012b). The uncertainty in this incandescence calibration is largely determined by the varying sensitivity of the instrument to different types of BC, which is around  $\pm 14\%$  (Laborde et al., 2012a). Laborde et al. (2012b) also showed that a 9% uncertainty in the accuracy of any individual incandescence calibration is reasonable, based on multiple calibrations with multiple instruments. The uncertainty in the mass and scattering cross-section of any individual particle is larger than these numbers, but this only serves to widen the measured distributions and has a minimal impact on the average properties of the particles or the integrated distributions.

#### AMS concentrations

The AMS chemical species measurements are used to calculate the density and refractive index of the BC coatings. The concentration,  $C_{\text{S}}$ , of a species, S, measured by the AMS scales with calibration factors described by Canagaratna et al. (2007):

$$C_{\text{S}} \propto \frac{1}{\text{IE}_{\text{NO}_3}} \frac{1}{\text{RIE}_{\text{S}}} \frac{1}{\text{CE}} \frac{1}{Q},$$

30 where  $IE_{NO_3}$  is the ionisation efficiency of  $NO_3$ ,  $RIE_S$  is the relative ionisation efficiency of the species in question, CE is the collection efficiency, and Q is the flowrate.

Bahreini et al. (2009) summarised the uncertainties associated with these factors based on previous literature available at the time. It is conventional in the AMS community to quote  $2\text{-}\sigma$  uncertainties, so the standard deviation is half these values. The  $2\text{-}\sigma$  uncertainties on  $IE_{NO_3}$  and  $RIE_{NH_4}$  are both  $\sim 10\%$ , taken from the ammonium nitrate calibrations. The  $2\text{-}\sigma$  uncertainties on  $RIE_{SO_4}$  and  $RIE_{OA}$  are 15% and 20%. As we have used the composition-dependent parametrisation to calculate CE (Middlebrook et al., 2012), the  $2\text{-}\sigma$  uncertainty on CE is around 30%. The scale factors for each species are then

5  $\kappa_{NO_3} = \kappa_{IE_{NO_3}} \times \kappa_{CE} \times \kappa_{TE}$

$$\kappa_{OA} = \kappa_{IE_{NO_3}} \times \kappa_{RIE_{OA}} \times \kappa_{CE} \times \kappa_{TE}$$

$$\kappa_{SO_4} = \kappa_{IE_{NO_3}} \times \kappa_{RIE_{SO_4}} \times \kappa_{CE} \times \kappa_{TE}$$

$$\kappa_{NH_4} = \kappa_{IE_{NO_3}} \times \kappa_{RIE_{NH_4}} \times \kappa_{CE} \times \kappa_{TE}$$

Using this method, the resultant  $2\text{-}\sigma$  uncertainties on  $NO_3$ , OA,  $SO_4$  and  $NH_4$  mass concentrations are 33%, 39%, 37% and  
10 36% respectively, which compare well to the numbers provided by Bahreini et al. (2009).

### Assumed properties of organic aerosol

The composition-dependent calculations of the coating density and refractive index require knowledge of the properties of the aerosol components. For inorganic aerosol these are fairly well known, but the variable composition of OA means its properties can vary. For density we use the values determined by Cross et al. (2007) of  $1.77 \text{ g cm}^{-3}$  for inorganics and  $1.2 \text{ g cm}^{-3}$  for  
15 organics. These values were successfully used by Cross et al. (2007) in a comparison of light scattering to aerodynamic size using the AMS composition to calculate density. The uncertainty in the OA density is not immediately obvious, but a value of  $\pm 0.1 \text{ g cm}^{-3}$  seems appropriate based on previous literature (e.g. Kroll et al., 2009).

For the coating refractive index, we use a top-down approach. Previous work has often used a value of  $1.5 + 0i$  (e.g. Schwarz et al., 2008; Taylor et al., 2015; Liu et al., 2015, 2017), and Taylor et al. (2015) also showed that this is a small sensitivity to the  
20 determination of particle size. Assuming a 9% BC mass fraction of the total submicron aerosol (Wu et al., 2020), volume mixing assuming  $m_{BC} = 1.85 - 0.71i$  then gives an effective refractive index with a real component of 1.53. This value compares well with previous estimates by Haywood et al. (2003) and Peers et al. (2019), who found 1.54 and 1.51 respectively by comparing to bulk optical measurements. Comparing to the range of effective refractive index values found in previous studies of biomass burning (Guyon et al., 2003; Sayer et al., 2014), an uncertainty in the real component of the coating refractive index of 0.04 is  
25 a good conservative estimate.

### Monte Carlo Results

Table S2 shows the results of the Monte Carlo analysis in terms of physical properties of the particles. The uncertainties in the derived coating thicknesses are around  $\pm 8\%$ . A comparison by Laborde et al. (2012b) showed that the whole range from different SP2 instruments was contained within  $\pm 17\%$ , which could be considered representative of a  $2\text{-}\sigma$  uncertainty, and so  
30 compares very well with our estimate. The uncertainty in MR is larger, probably due to the uncertainty in the coating density.



**Table S2.** Mean and standard deviation of physical parameters involved in the Monte Carlo analysis of different optical models.

	<b>Mean</b>	<b>Standard deviation</b>
Median shell/core diameter ratio	2.33	0.15
Median MR	8.7	1.8
Median coating thickness (nm)	86	7

Table S3 shows the outputs of the Monte Carlo analysis. For the output of the optical models in terms of MAC and AAE, the derived uncertainties are in the range 2 – 12%. We suspect that, when using a polydisperse BC distribution, competing effects of varying the input parameters cancel out, reducing the uncertainty of the optical properties compared to the physical properties.

**Table S3.** Monte Carlo relative standard deviations of bulk absorption parameters using different optical schemes. For the optical models that have a dependence on  $m_{BC}$  (Core/shell, CS- $E_{Abs}$  volume mixing, Maxwell-Garnett and Bruggemann), the average value is listed here.

	Core/shell	CS- $E_{Abs}$	Volume mixing	Maxwell-Garnett	Bruggemann	Liu- $E_{Abs}/Sca$	Chak-MAC	Chak- $E_{Abs}$	Wu- $E_{Abs}$
MAC 405 nm	0.07	0.04	0.12	0.12	0.12	0.04	0.07	0.07	0.03
MAC 514 nm	0.06	0.04	0.11	0.11	0.11	0.05	0.07	0.07	0.04
MAC 655 nm	0.05	0.05	0.11	0.11	0.11	0.05	0.07	0.07	0.04
AAE <sub>405/514</sub>	0.09	0.03	0.09	0.09	0.09	0.03	0	0	0.03
AAE <sub>514/655</sub>	0.07	0.03	0.07	0.07	0.07	0.02	0	0	0.03

## S4 Skin-depth shielding in Mie models

In the geometric optics regime, the absorption cross-section of a black sphere is the same as its geometric cross-section,  $\pi r^2$ , where  $r$  is the radius. This cross-section is independent of wavelength. In Mie theory, absorbing spheres asymptote to the geometric optics regime when they are sufficiently large and sufficiently absorbing. A useful concept to illustrate this transition is the optical skin depth, defined as  $\delta = \lambda / (2\pi k_{\text{BC}})$  (Hecht, 2014), where  $k_{\text{BC}}$  is the imaginary component of  $m_{\text{BC}}$ . This is the distance over which the intensity of light penetrating an absorbing medium drops by a factor of  $1/e$ . For clarity, this skin depth is not related to coatings in the core/shell model- it is simply the part of a homogeneous absorbing sphere that is near

5 the surface. For small spheres the skin depth is not an issue, but when they become similar in size to the skin depth, the centre of the sphere is essentially shielded by the surface, and is therefore less effective at absorbing incident light. When the sphere becomes large enough, the centre receives little to no light, and only the region near the surface of the particle is able to absorb light. The absorption therefore scales with cross-section rather than volume, and the MAC scales inversely with diameter. This 'skin-depth shielding' is strongest for larger particles, high values of  $k_{\text{BC}}$ , and shorter wavelengths.

10 This wavelength dependence causes the underprediction of MAC for the core/shell Mie model in Fig. 6 at 405 nm, but not at longer wavelengths. Figure S4 shows example calculations of MAC for uncoated BC particles, as well as coated. Particles with BC cores of 185 nm (the average MMD measured during CLARIFY) fall within the geometric optics regime at a wavelength of 405 nm, but not at 655 nm. Therefore, for this size of particle, the skin-depth shielding reduces the blue MAC but not the red. The presence of coatings modifies the shape and magnitude of the MAC curves in Fig. S4, but it does not change the

15 overall concept. These calculations were carried out with nonabsorbing coatings, confirming that this is an effect of Mie theory and not related to BrC. The wavelength dependence of the skin-depth shielding is the reason the Mie calculations have AAE values below 1 (shown in Fig. 7), and the stronger effect at higher values of  $k_{\text{BC}}$  causes a lower AAE.

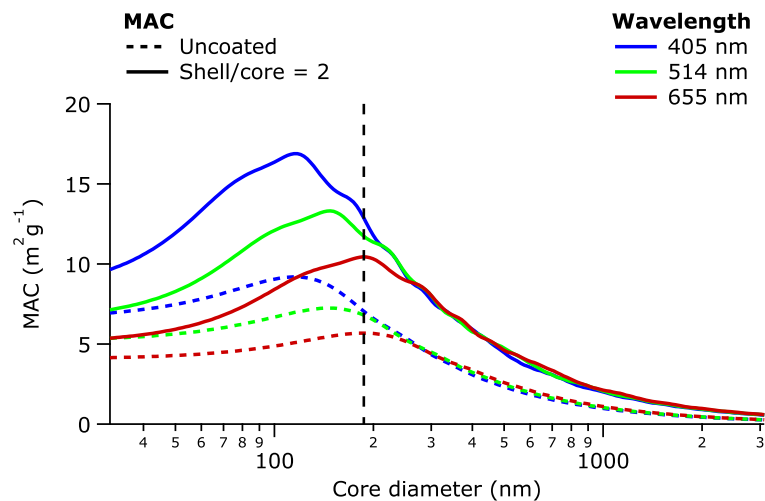


**Figure S4.** MAC for different core diameters, using the Mie core/shell model. Calculations were performed using  $m_{BC} = (1.85 - 0.71)i$ . The vertical dashed line is at 185 nm, which is similar to the average MMD in CLARIFY shown in Fig. 3.

### S5 Impact of $m_{BC}$ on MAC for typical particles

Figure S5 shows core/shell MAC and AAE calculations with core and shell diameters calculated using typical core/shell particles; the  $D_C$  distribution taken from Fig. 5a, and representative shell/core ratios of 2.4. Example  $m_{BC}$  values follow the rule of  $n_{BC} = k_{BC} + 1$ , where  $n_{BC}$  and  $k_{BC}$  are the real and imaginary components of  $m_{BC}$ . A value of  $1.5 - 0i$  was also used for the shell refractive index. This figure is discussed further in Sect. 5.2.

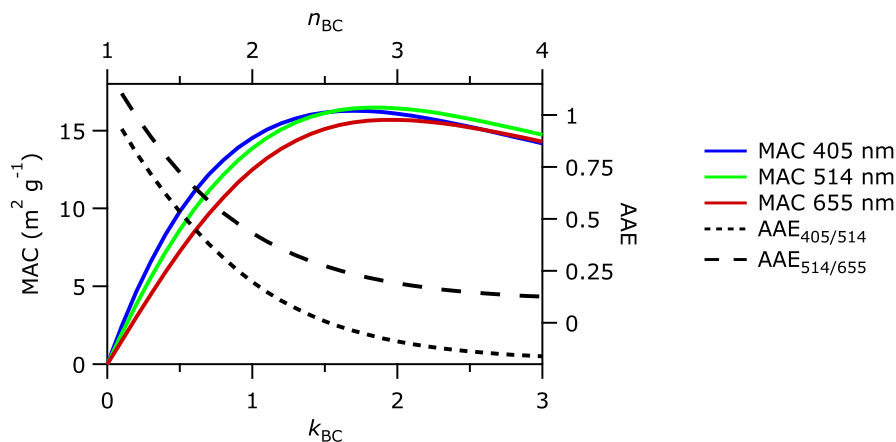


**Figure S5.** MAC and AAE as a function of  $m_{BC}$  for typical core/shell particles measured during CLARIFY.